Annular Modes in the Extratropical Circulation. Part II: Trends*

DAVID W. J. THOMPSON AND JOHN M. WALLACE

Department of Atmospheric Sciences, University of Washington, Seattle, Washington

GABRIELE C. HEGERL

Joint Institute for the Study of the Atmosphere and Ocean, University of Washington, Seattle, Washington

(Manuscript received 1 February 1999, in final form 1 July 1999)

ABSTRACT

The authors exploit the remarkable similarity between recent climate trends and the structure of the ''annular modes'' in the month-to-month variability (as described in a companion paper) to partition the trends into components linearly congruent with and linearly independent of the annular modes.

The index of the Northern Hemisphere (NH) annular mode, referred to as the Arctic Oscillation (AO), has exhibited a trend toward the high index polarity over the past few decades. The largest and most significant trends are observed during the ''active season'' for stratospheric planetary wave–mean flow interaction, January–March (JFM), when fluctuations in the AO amplify with height into the lower stratosphere. For the periods of record considered, virtually all of the JFM geopotential height falls over the polar cap region and the strengthening of the subpolar westerlies from the surface to the lower stratosphere, ~50% of the JFM warming over the Eurasian continent, ~30% of the JFM warming over the NH as a whole, ~40% of the JFM stratospheric cooling over the polar cap region, and ~40% of the March total column ozone losses poleward of 40°N are linearly congruent with month-to-month variations in the AO index. Summertime sea level pressure falls over the Arctic basin are suggestive of a year-round drift toward the positive polarity of the AO, but the evidence is less conclusive. Owing to the photochemical memory inherent in the ozone distribution, roughly half the ozone depletion during the NH summer months is linearly dependent on AO-related ozone losses incurred during the previous active season.

Lower-tropospheric geopotential height falls over the Antarctic polar cap region are indicative of a drift toward the high index polarity of the Southern Hemisphere (SH) annular mode with no apparent seasonality. In contrast, the trend toward a cooling and strengthening of the SH stratospheric polar vortex peaks sharply during the stratosphere's relatively short active season centered in November. The most pronounced SH ozone losses have occurred in September–October, one or two months prior to this active season. In both hemispheres, positive feedbacks involving ozone destruction, cooling, and a weakening of the wave-driven meridional circulation may be contributing to a delayed breakdown of the polar vortex and enhanced ozone losses during spring.

1. Introduction

In the companion paper, Thompson and Wallace (2000, hereafter Part I) document the remarkable similarity between the leading modes of month-to-month variability of the extratropical general circulation in the Northern and Southern Hemispheres. Both can be characterized as ''annular modes'' involving

- ''seesaws'' in atmospheric mass between the polar cap regions poleward of 60° lat and the surrounding zonal rings centered near 45° lat, as manifested in the respective leading empirical orthogonal functions (EOFs) of the sea level pressure (SLP) field;
- out-of-phase variations in westerly momentum in the ~35° and ~60° lat belts; and
- strong perturbations in temperature and total column ozone over the polar cap region during the stratosphere's active seasons that appear to be related to fluctuations in the intensity of the wave-driven meridional circulation.

Various indices related to the Northern Hemisphere (NH) annular mode have exhibited a pronounced drift toward the high index polarity during the past few decades, which is reflected in patterns of sea level pressure, geopotential height, and surface air temperature trends (Hurrell 1995, 1996; Graf et al. 1995; Thompson and Wallace 1998, hereafter TW98). Trends that resemble the Southern Hemisphere (SH) annular mode have been

* JISAO Contribution Number 689.

Corresponding author address: Dr. David W. J. Thompson, Joint Institute for the Study of the Atmosphere and Ocean, University of Washington, Box 354235, Seattle, WA 98195-4235.
E-mail: davet@atmos.washington.edu

documented by Hurrell and van Loon (1994), Chen and Yen (1999), and Randel and Wu (1999). In this paper we document the similarity between the annular modes and the trends in greater detail, drawing upon the description of the month-to-month variability of the annular modes presented in Part I.

The next section describes the datasets used in this study and the analysis technique used to estimate the component of the observed trends that is ''linearly congruent'' with the time variations in the annular modes. In section 3 we partition the NH wintertime (January–March) trends in surface air temperature, precipitation, total column ozone, tropopause pressure, and the zonal-mean circulation into components that are linearly congruent with and linearly independent of the Arctic Oscillation (AO) index. In section 4 we document the seasonality of the NH trends and the degree to which an AO-like signature is evident in trends throughout the year. Less clearly defined SH trends and their relation to the SH annular mode are the subject of section 5. In the final discussion section we offer an interpretation as to why the NH and SH annular modes are so prominent in both the month-to-month variability and the trends, and why they are so similar to one another despite the marked differences in the background climatologies of the two hemispheres.

2. Data and analysis techniques

Several monthly mean, gridded datasets are used in this study: surface air temperature (SAT) was provided by P. D. Jones at the University of East Anglia (Jones 1994; Parker et al. 1995); SLP from the data support section at the National Center for Atmospheric Research (NCAR) (Trenberth and Paolino 1980); precipitation by M. Hulme at the University of East Anglia (Hulme 1992, 1994); lower-stratospheric temperature data, derived from the Microwave Sounding Unit Channel 4 (MSU-4), obtained from the National Aeronautics and Space Administration (NASA) Marshall Space Flight Center (Spencer and Christy 1993); total column ozone, derived from the *Nimbus-7* total ozone mapping spectrometer (TOMS), from the NASA Goddard Space Flight Center; and monthly mean fields of the National Oceanic and Atmospheric Administration (NOAA) National Centers for Environmental Prediction (NCEP)–NCAR reanalysis (Kalnay et al. 1996) from the NOAA Climate Diagnostics Center.

Following Part I, fluctuations in the polarity of the AO are defined on the basis of the standardized leading principal component time series of monthly mean NH (defined herein as poleward of 20°N) SLP for all months of the year. We refer to this time series as the AO index: positive values of the index correspond to negative height anomalies over the polar cap, and vice versa. The structure of this mode in the month-to-month variability is documented in TW98 and in Part I. SLP anomalies are expressed in terms of meters of the equivalent 1000-hPa geopotential height anomalies as inferred from the approximate relationship $Z_{1000} \cong 8(\text{SLP} - 1000\ \text{hPa})$, where Z_{1000} is the height of the 1000-hPa surface.

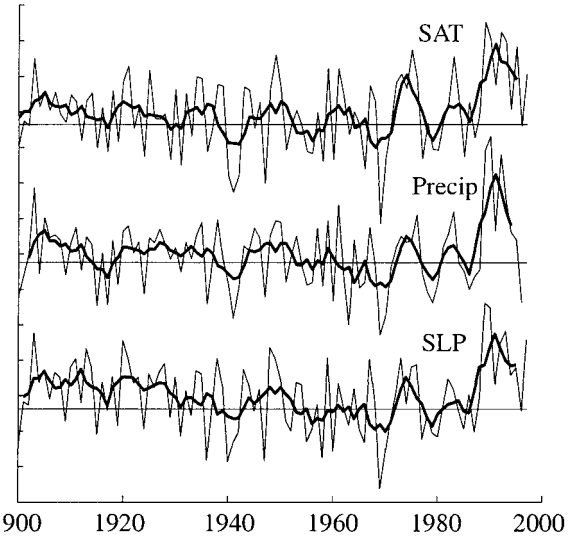

FIG. 1. Standardized JFM proxy AO indices based on SAT, precipitation, and SLP. Correlation statistics are presented in Table 1. Light lines indicate JFM seasonal means; heavy lines indicate 5-yr running means. The interval between tick marks on the vertical axis is one standard deviation.

The observed trends are partitioned into linearly congruent and linearly independent (or residual) components with respect to the monthly AO index in the following manner.

1) Total linear trends are estimated as the slope of a straight line fitted (in a least squares sense) to the observed data at each grid point based on the reference periods defined in the next section.
2) The component of the trends that is linearly congruent with the monthly AO index is estimated at each grid point by (a) regressing monthly values of that grid point's time series onto the AO index, and then (b) multiplying the resulting regression coefficient by the linear trend in the AO index. Note that the fraction of the trend in standardized time series $x(t)$ that is linearly congruent with the AO index is equivalent to the correlation coefficient between $x(t)$ and the AO index times the ratio of the trend in the AO to the trend in $x(t)$.
3) The component of the trends that is linearly independent of the AO index is obtained by subtracting 2) from 1). For brevity these patterns will be labeled ''AO residual'' trends.

3. Recent Northern Hemisphere wintertime trends

In Part I we showed that AO-related variance is largest in both the NH troposphere and lower stratosphere during the NH winter months January–March (JFM). Figure 1 shows standardized proxy indices of the AO for these ''active'' season months based on three independent data

TABLE 1. Correlation coefficients between the AO proxy time series shown in Fig. 1. Correlations are based on 1947–96 JFM seasonal (monthly) mean values.

	SAT	Precip
SLP	0.92 (0.87)	0.88 (0.86)
SAT		0.85 (0.80)

sources: SLP, SAT, and precipitation. Each dataset's time series was constructed by 1) forming the correlation map based on the AO index, as defined in section 2, using JFM monthly mean data (1958–97, 20°–90°N), and then 2) projecting the JFM monthly mean data onto this correlation pattern for the extended period of record, 1900–97. In order to minimize the influence of the global warming trend upon the SAT index, the hemispheric-mean value was removed from each grid point before that calculation was performed. (In practice, the influence of this correction upon the resulting index proved to be small.) All three indices are strongly correlated with each other on month-to-month and interannual timescales (Table 1) and hence are indicative of fluctuations in the AO. The most pronounced feature in all three of them is a conspicuous trend over the past few decades that appears to be unprecedented in the historical record. Here in Part II, the signature of this trend in the climate of the NH is documented. Most of the results are based on the 30-yr reference period 1968–97. This particular choice was dictated by the fact that results based on shorter periods of record are more sensitive to small changes in the trend length, while results for periods much longer than this range tend to obscure the recent secular behavior of the AO. For the satellite data, trends are estimated based on the full available period of record, 1979–97, unless otherwise noted.

a. Wintertime trends in the lower troposphere

Figure 2 (top) shows 30-yr (1968–97) JFM linear trends in SLP and SAT. As demonstrated in TW98 for the longer winter season November–April, and consistent with the findings of Walsh et al. (1996), recent trends in SLP are dominated by falling heights over the Arctic basin, locally as large as 70 m $(30\ \text{yr})^{-1}$. Recent trends in NH wintertime SAT are dominated by strong warming over the high-latitude continents with maximum values as high as 5 K $(30\ \text{yr})^{-1}$ over parts of Siberia, and weaker cooling over Greenland and Labrador (see also Jones 1994; Parker et al. 1996; Nicholls et al. 1996; Hurrell 1995, 1996).

The structural similarity between trends in SLP and SAT and the corresponding signatures of the AO, shown in the middle panels of Fig. 2, is striking. Virtually all of the SLP falls over the Arctic basin, roughly half of the warming over Siberia, and all of the cooling over eastern Canada and Greenland are linearly congruent with the monthly time series of the AO. The AO residual trends (Fig. 2, bottom) are weaker and more spatially amorphous, with warming over most of the hemisphere. The most conspicuous regional features in the residual trends are the SLP falls over the North Pacific, which occur in conjunction with warming over western Canada and Alaska. ''ENSO-like'' interdecadal variability, as documented in Trenberth and Hurrell (1994) and Zhang et al. (1997) has contributed to these features. The ENSO-related pressure drop over the North Pacific can be attributed to the abrupt 1976–77 ''regime shift'' discussed in those papers. Apart from that feature, SLP over the North Pacific has risen slightly during the past 30 yr, consistent with the trend toward the ''high index'' state of the AO during this period. The juxtaposition of ENSO-like and AO-related SLP variability over the North Pacific has also been discussed by Volodin and Galin (1998), who offer a similar interpretation.

Based on the above analysis, ~0.3 K of the 1.0 K JFM warming of the NH poleward of 20°N over the past 30 yr is linearly congruent with the monthly time series of the AO. Consistent with model simulations of the response to increasing greenhouse gases and sulfate aerosols (e.g., Kattenberg et al. 1996; Mitchell et al. 1995; Mitchell and Johns 1997; Cubasch et al. 1996), AO residual trends are larger over the continents than over the surrounding oceans in JFM (1.1 vs 0.4 K) and they are larger during JFM than in the annual average (1.1 vs 0.7 K). More complete statistics are presented in Table 2.

Precipitation trends for the period 1968–96 [expressed as percent departures from the JFM climatology $(29\ \text{yr})^{-1}$] are shown in the top panel of Fig. 3. The most pronounced features are the increases over northern Europe, Alaska, northern Mexico, and central China, and the decreases over central North America, southern Europe, and eastern Asia. The signature of the AO in the NH precipitation field, shown in the bottom panel of Fig. 3, is almost identical to the pattern of precipitation anomalies associated with the North Atlantic Oscillation (NAO) (Hurrell 1995; Hurrell and van Loon 1997; Dai et al. 1997) not only over Europe, but over much of the hemisphere. As documented in Table 3, a large fraction of the precipitation trend in the regions where they are most pronounced is linearly congruent with the monthly AO time series.

b. Wintertime trends in the lower stratosphere

Figures 4–6 show total, AO congruent, and AO residual trends in 50-hPa height (Z_{50}), MSU-4 temperature (indicative of the layer extending from ~150 to ~50 hPa), TOMS total column ozone, and tropopause pressure. Trends in Z_{50} and tropopause pressure are based on the 30-yr period 1968–97. Trends in TOMS and MSU-4 are estimated based upon the available period of record: November 1978–April 1993 for TOMS and 1979–97 for MSU-4, and are expressed as incremental changes per 15 and 19 yr, respectively. Because TOMS instrumentation requires insolation in order to function,

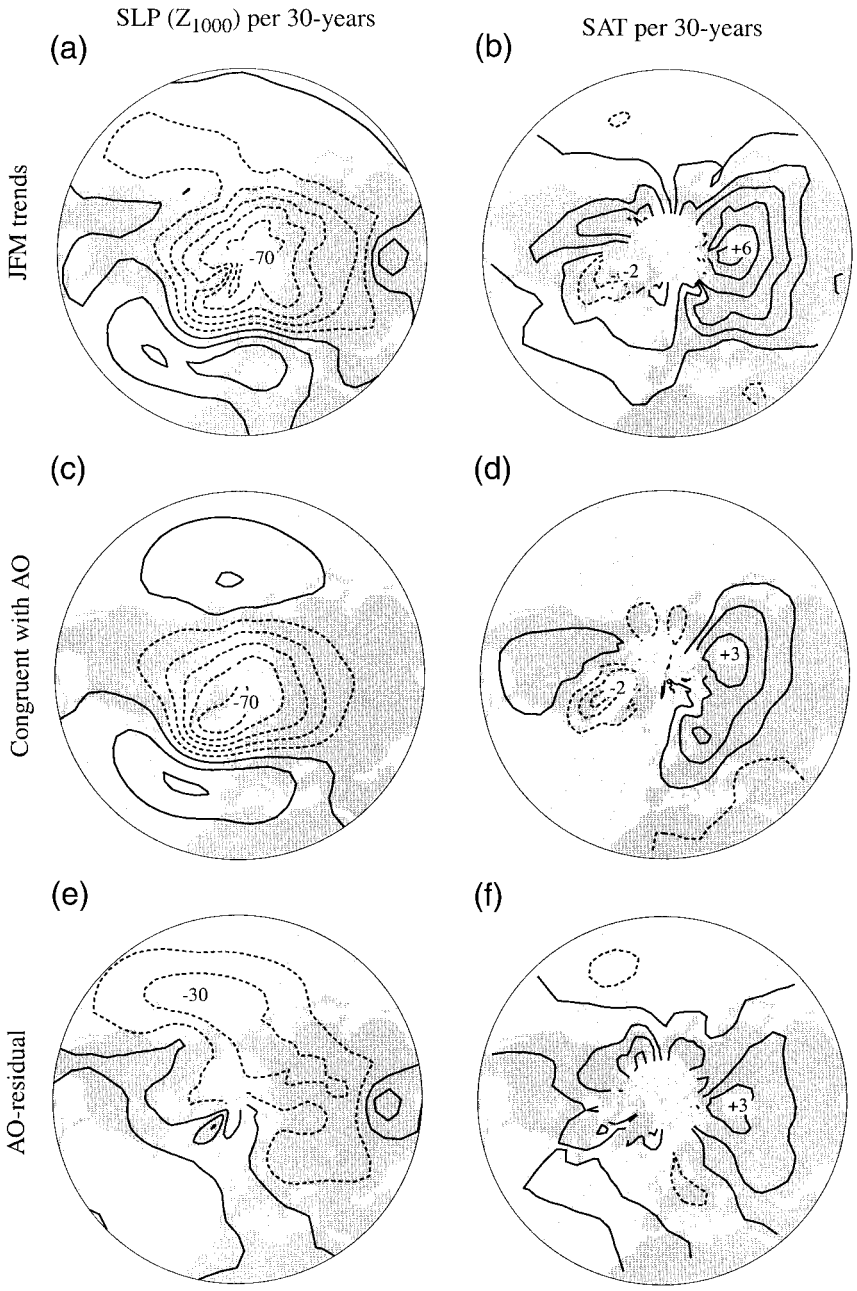

FIG. 2. 30-yr (1968–97) linear JFM trends in (left) SLP expressed as 1000-hPa geopotential height, Z_{1000}, and (right) SAT. (top) Total trends. (middle) The components of the trends that are linearly congruent with the monthly AO index (as defined in section 2). (bottom) AO residual trends. Contour intervals are 15 m (30 yr)$^{-1}$ (-22.5, -7.5, $+7.5$, . . .) for SLP and 1 K (30 yr)$^{-1}$ (-1.5, -0.5, $+0.5$, . . .) for SAT.

total column ozone is mapped only for the month of March when the spatial coverage extends nearly to the pole.

Total trends in Z_{50} and MSU-4 temperature (Fig. 4, top) are predominantly zonally symmetric. Consistent with the findings of Randel and Wu (1999), geopotential height falls of ~250 m (30 yr)$^{-1}$ and cooling of ~5 K (19 yr)$^{-1}$ are evident over broad regions of the polar cap, indicative of a substantial strengthening of the polar vortex in the lower stratosphere. The AO congruent component (Fig. 4, middle panels) accounts for ~40% of the cooling and ~70% of the geopotential height falls poleward of 60°N in the lower stratosphere. An even larger fraction of the trends in these fields is linearly congruent with the leading PC of the monthly mean, zonal-mean geopotential height field from 20° to 90°N,

TABLE 2. 30-yr (1968–97) linear trends in NH surface air temperature [K(30-yr^{-1})] and the component of the trends that is linearly congruent with the monthly AO index (as defined in section 2).

	Land + ocean (20°–90°N)	Land (20°–90°N)	Eurasian land (40°–70°N, 0°–140°E)
JFM total trend	+1.0	+1.7	+3.0
JFM trends congruent with AO	+0.3	+0.6	+1.6
JFM AO residual trend	+0.7	+1.1	+1.4
Annual mean total trend	+0.6	+0.8	+1.1
Annual mean AO residual trend	+0.5	+0.7	+0.8

1000–50 hPa (as in Fig. 3 of Part I, hereafter denoted AO*). The corresponding AO* congruent and AO* residual trends are shown in Fig. 5.

March ozone trends in data from the TOMS from 1979 to 1993 (Fig. 6a) are indicative of a thinning of the ozone layer over the entire NH, with losses of up to 110 Dobson units (DU) over Siberia versus minimal losses over the Davis Strait region. The trend averaged over the region poleward of 40°N is −49 DU (~12% of the climatological-mean value) (15 yr)$^{-1}$. The AO congruent component accounts for much of the horizontal structure in these trends and for ~40% of the area averaged losses poleward of 40°N. This fraction is comparable to the fraction of observed NH ozone trends that cannot be explained by photochemical processes alone in atmospheric models (World Meteorological Organization 1995).

Owing to the strong vertical gradient of ozone in the vicinity of the tropopause, tropopause pressure tends to be positively correlated with total column ozone and, in this sense, may be viewed as a proxy for it (e.g., Steinbrecht et al. 1998). As noted in Part I, the total column ozone structure congruent with the AO time series is a reflection of anomalies in tropopause pressure associated with the baroclinic planetary wave signature embedded within the annular mode. In contrast to total column ozone, tropopause pressure based on the NCEP–NCAR reanalyses, shown in the right-hand panel of Fig. 6, is available during all calendar months and for the full 30-yr record. The AO signatures in total column ozone and tropopause pressure (middle panels) appear to be consistent: the high index state of the AO favors increased total column ozone and a depressed tropo-

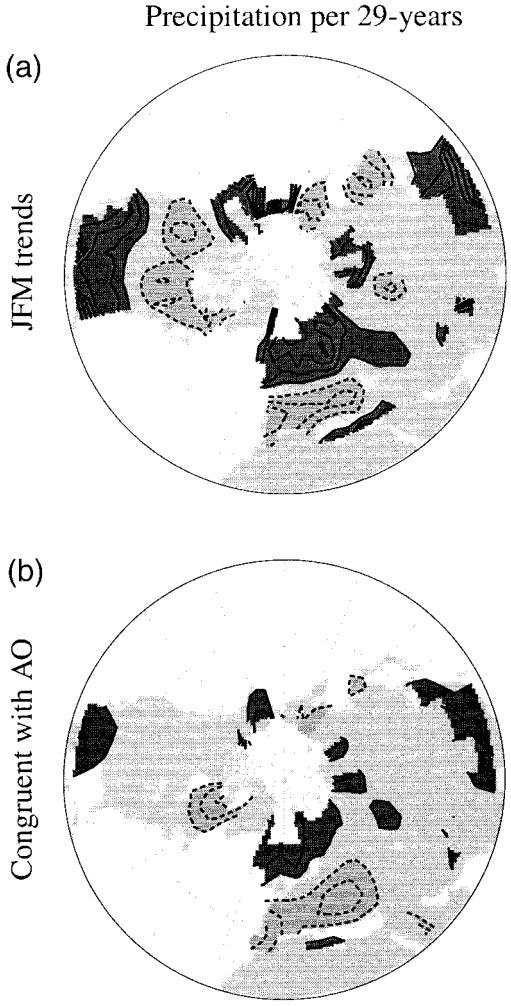

FIG. 3. (top) 29-yr (1968–96) linear Jan–Mar (JFM) trends in precipitation [% of JFM climatology (29 yr)$^{-1}$] and (bottom) the components of the trends that are linearly congruent with the monthly AO index. Contour intervals are 10% (29 yr)$^{-1}$ (−10, 10, 20, . . .). Dark shading indicates increased precipitation of at least +10%; light shading indicates reduced precipitation of at least −10%. The zero contour line is omitted and negative contours are dashed.

TABLE 3. 29-yr (1968–96) linear trends in JFM precipitation [% of JFM climatology (29 yr^{-1})], the trends that are linearly congruent with the monthly AO index, and the correlation coefficients between JFM monthly precipitation time series and the AO index (the 99% confidence level is ~0.22).

Region	Total trend	Congruent with AO	*r* (month-to-month)
Norway (55°–65°N; 5°–10°E)	+45%	+37%	0.62
Scotland (55°–60°N; 350°–355°E)	+51%	+32%	0.59
Spain 35°–45°N; 350°–0°E)	−49%	−33%	0.53
Balkans (45°–50°N; 15°–30°E)	−31%	−31%	0.66
Central China (25°–40°N; 105°–110°E)	+29%	+22%	0.48

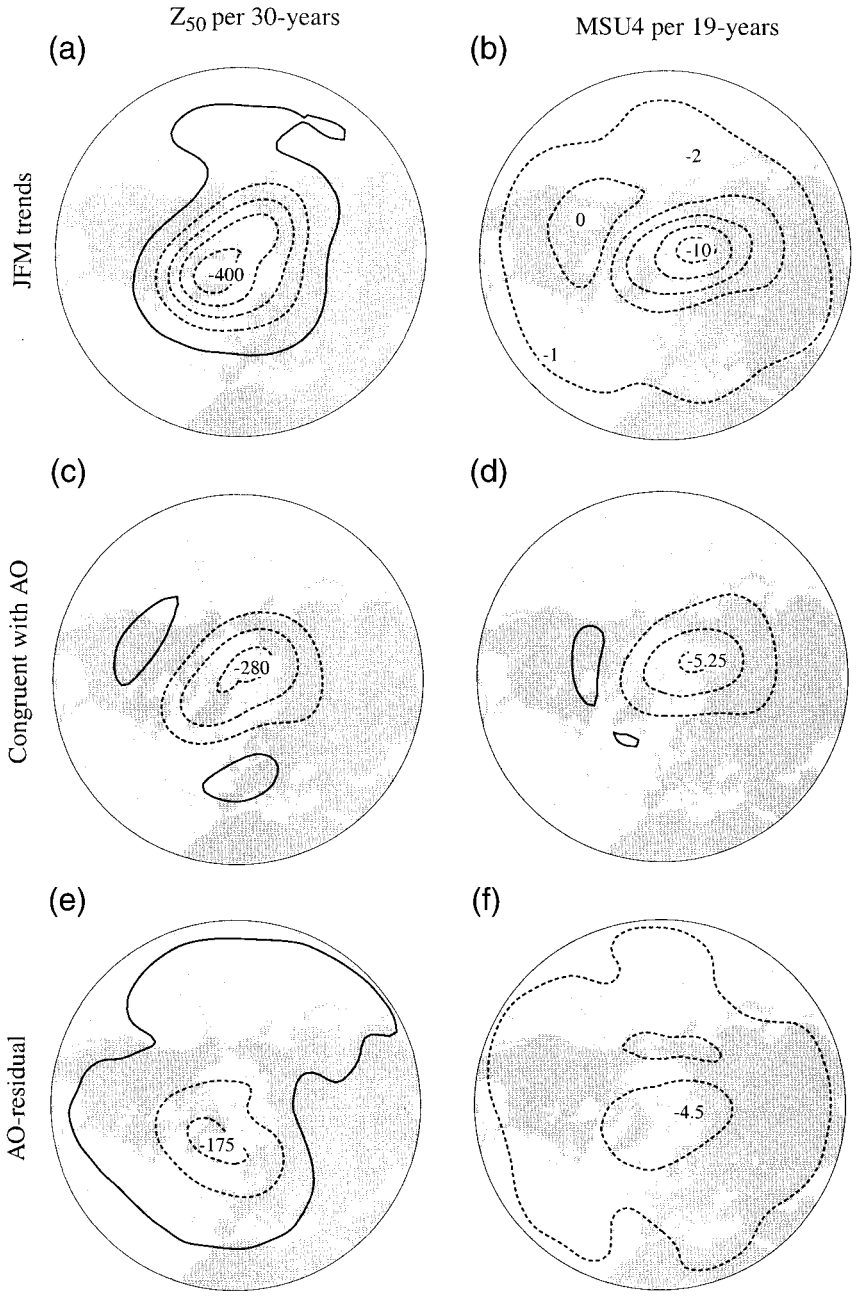

FIG. 4. (left) 30-yr (1968–97) linear Jan–Mar (JFM) trends in 50-hPa height (Z_{50}) and (right) 19-yr (1979–97) linear trends in MSU-4 lower-stratospheric temperature. (top) Total trends. (middle) The components of the trends that are linearly congruent with the monthly AO index. (bottom) AO residual trends. Contour intervals are 100 m (30 yr)$^{-1}$ (-150, -50, $+50$, . . .) for Z_{50} and 2 K (19 yr)$^{-1}$ (-3, -1, 1, . . .) for MSU-4 temperature.

pause near the southern tip of Greenland and changes in the opposite sense over the Siberian Arctic. The AO signature is clearly evident in the total trends in tropopause pressure (top right panel): ~40% of the 16-hPa decrease in tropopause pressure averaged over the region poleward of 60°N during JFM from 1968 to 1997 is linearly congruent with month-to-month variations in the AO. In contrast to the AO congruent trends, the AO residual trends in total column ozone and tropopause pressure do not appear to be linearly related in the spatial domain.

The above analysis of the TOMS data was repeated using the AO* index. The resulting patterns (not shown) are virtually indistinguishable from those in Fig. 6.

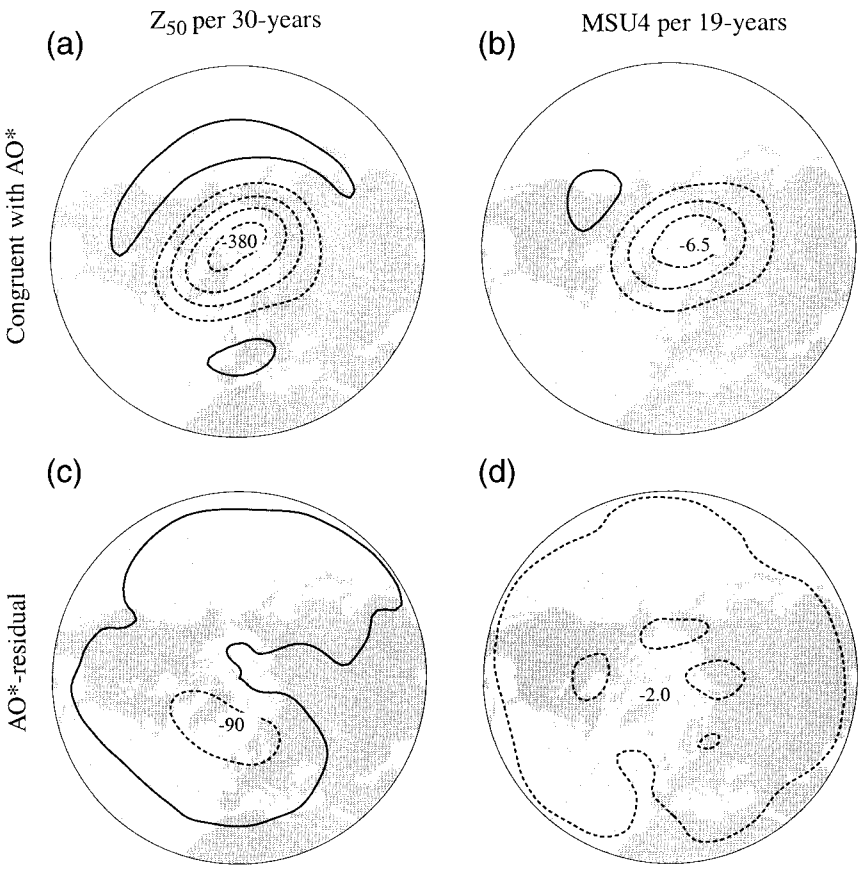

FIG. 5. As in the middle and bottom panels of Fig. 4, but for the (top) components of the trends that are linearly congruent with the monthly AO* index and (bottom) the components that are linearly independent of the monthly AO* index. The AO* index is the leading PC of the zonal-mean geopotential height field.

Thus, the results in Fig. 6, including the rather large residual trends, are not highly sensitive to the manner in which the AO is defined.

c. Wintertime trends in the zonal-mean circulation and temperature fields

Consistent with trends in zonally varying SLP (Fig. 2) and 50-hPa height (Fig. 4), 30-yr trends in JFM zonal-mean zonal wind (Fig. 7a) are characterized by a strengthening of the westerly flow poleward of 45°N from the surface to the lower stratosphere and a weakening of the westerlies in the troposphere to the south of 45°N: the westerlies near 55°N have increased by ~1–2 m s^{-1} near the surface and by as much as 10 m s^{-1} at the 50-hPa level. The corresponding 30-yr zonal-mean temperature trends in the NCEP–NCAR reanalyses are shown in the top right panel of Fig. 7. The polar lower stratosphere has cooled by up to 6 K while the zone extending from the midlatitude troposphere to the subtropical tropopause has warmed. This out-of-phase relationship between temperature trends over the polar cap and the tropical tropopause is suggestive of a weakening of the meridional transport circulation in the lower stratosphere, a finding supported by observations from the *Upper Atmosphere Research Satellite* (Randel et al. 1999). However, the warming of the tropical tropopause may also be spurious: a manifestation of a discontinuity in the time series coincident with the introduction of satellite data into the analyses around 1978, as pointed out by Randel and Wu (1999). To avoid undue emphasis on this feature, we have not extended the sections into the Tropics. The 30-yr trends in the (zonal) mean meridional circulation, indicated by the arrows, are dominated by a circulation in the same sense as the Ferrell cell between 40° and 70°N, and a strengthening and northward extension of the Hadley cell.

Comparing the top and middle panels of Fig. 7, it is evident that the most prominent features of the observed trends are linearly congruent with the monthly AO time series. The residual temperature trends (Fig. 7, bottom) are suggestive of a more homogenous cooling throughout the stratosphere and warming throughout the troposphere. The sign reversal in residual temperature trends corresponds closely to the tropopause level, which ranges from ~100 hPa in the Tropics to ~300

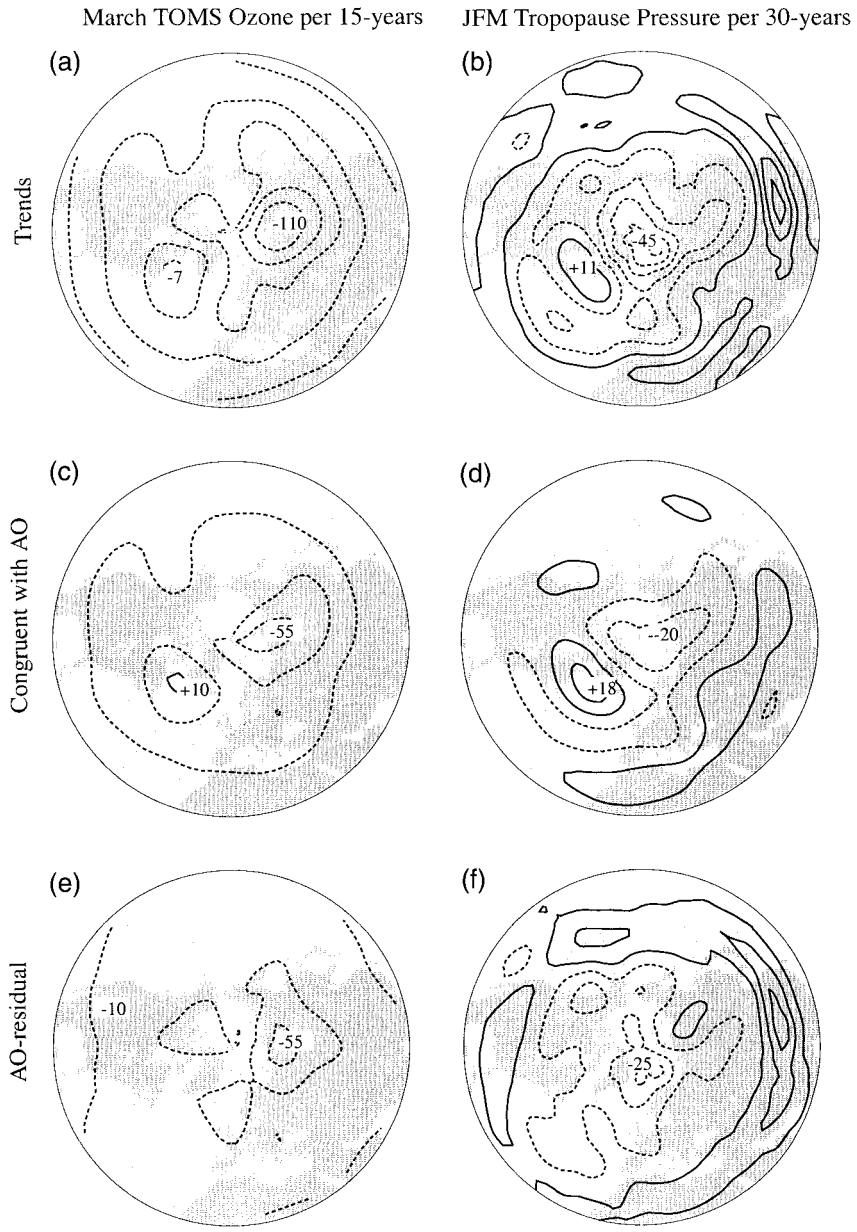

FIG. 6. 15-yr (1979–93) linear March trends in (left) total column ozone and (right) 30-yr (1968–97) linear JFM trends in tropopause pressure. (top) Total trends. (middle) The components of the trends that are linearly congruent with the monthly AO index. (bottom) AO residual trends. Contour intervals are 20 Dobson Units (DU) (15 yr)$^{-1}$ (-30, -10, $+10$, . . .) for TOMS total column ozone and 10 hPa (30 yr)$^{-1}$ (-15, -5, $+5$, . . .) for tropopause pressure.

hPa over the pole. Figure 8 shows corresponding results based on the AO* index. This redefinition of the annular mode slightly increases the amplitude of the linearly congruent component of the trends in the lower stratosphere and reduces the amplitude of the residuals. However, the most prominent features in the residual patterns (i.e., the nearly homogeneous cooling in the stratosphere and warming in the troposphere) are almost the same as in the previous figure.

The results shown in Figs. 2–8 indicate that substantial fractions of the recent trends in surface air temperature and total column ozone during the NH winter months are linearly congruent with the monthly AO time series. These trends are clearly reflected in JFM time series of Eurasian mean temperature and total column ozone at Arosa, Switzerland, shown together with the AO index in Fig. 9 for the period 1930–97. The Arosa time series is the longest continuous record of total column ozone

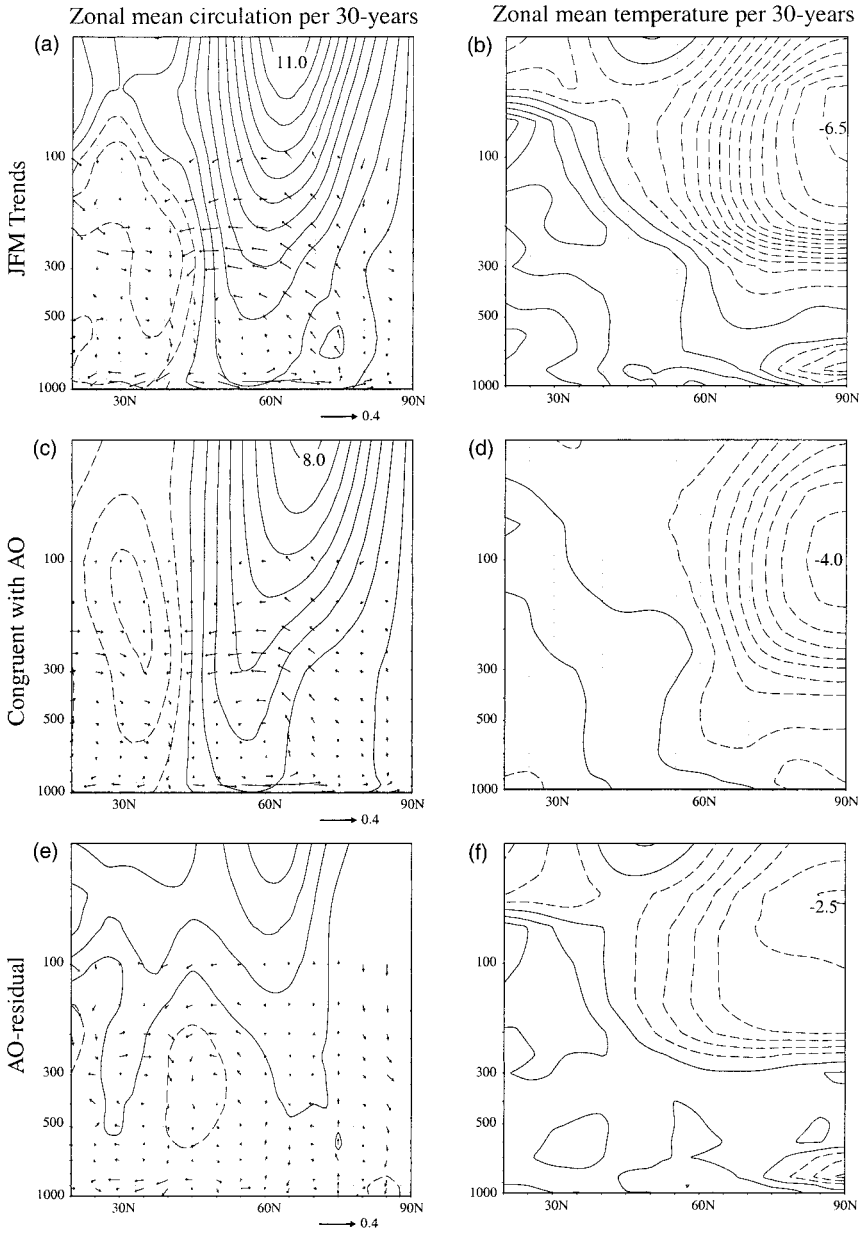

FIG. 7. 30-yr (1968–97) linear JFM trends in zonal-mean zonal wind (left, contours), meridional circulation (left, vectors), and (right) temperature. (top) Total trends. (middle) The components of the trends that are linearly congruent with the monthly AO index. (bottom) AO residual trends. Contour intervals are 1 m s^{-1} (30 yr)$^{-1}$ (-1.5, -0.5, $+0.5$, . . .) for zonal wind and 0.5 K (30 yr)$^{-1}$ (-0.75, -0.25, $+0.25$, . . .) for temperature. Vectors are m s^{-1} in the horizontal and cm s^{-1} in the vertical. Vector scale shown at bottom of figure.

(Staehelin et al. 1998). Although Switzerland is not centered near a prominent center of action of the AO signature in ozone (Fig. 6d), a strong correspondence between the two time series is evident on both interannual and interdecadal timescales. Based on this 68-yr record, variations in the AO account for 25% of the month-to-month variance and 43% of the year-to-year variance in JFM total column ozone over Arosa, and are linearly congruent with ~40% of the negative trend from 1968 to 1997. The corresponding percentages for Eurasian mean temperature are even higher.

4. Seasonality of recent Northern Hemisphere climate trends

Recent NH climate trends are most dramatic during JFM and the fraction of the trends that is linearly congruent with the AO is particularly large during those

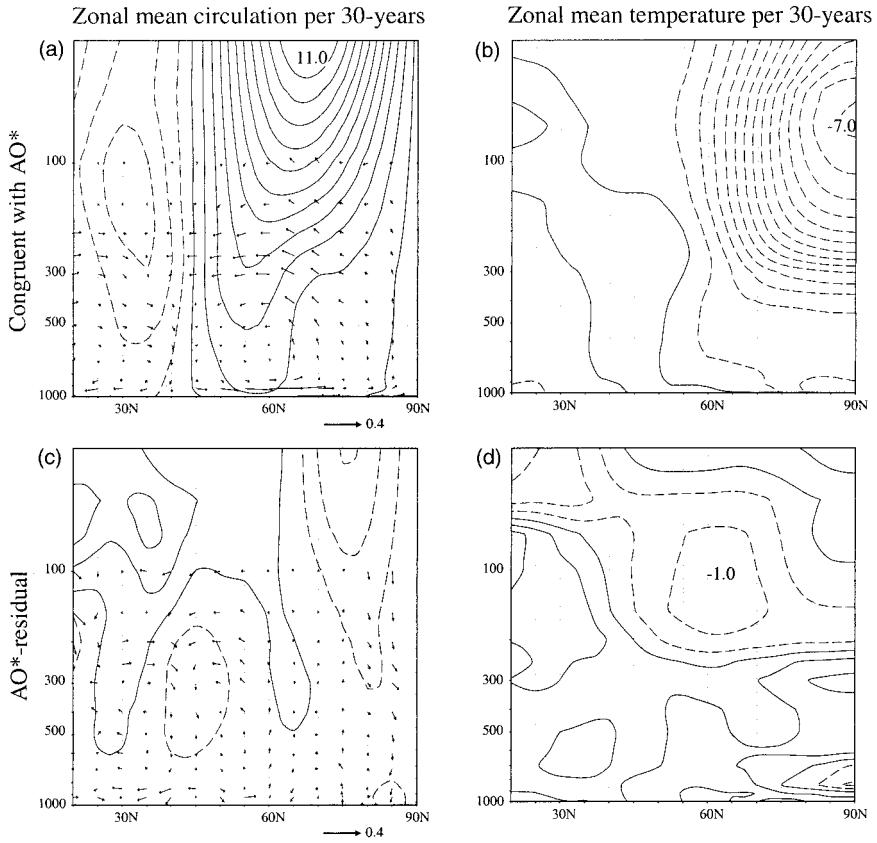

FIG. 8. As in the middle and bottom panels of Fig. 7, but for the components of the trends that are (top) linearly congruent with the monthly AO* index, and (bottom) the components that are linearly independent of the monthly AO* index.

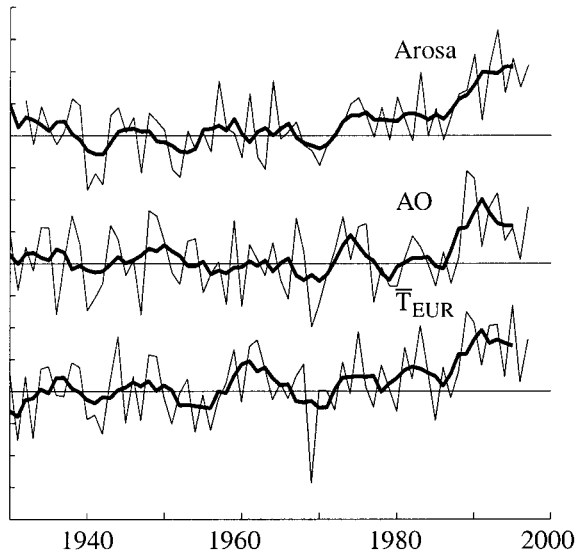

FIG. 9. Standardized JFM time series of (top) ground based ozone measurements from Arosa, Switzerland, inverted, (middle) the AO index and (bottom) Eurasian mean (40°–70°N, 0°–140°E) surface air temperature. Light lines indicate JFM seasonal means; heavy lines indicate 5-yr running means. The interval between tick marks on the vertical axis is one standard deviation.

same months. For the sake of completeness we include here a brief summary of results for other seasons, with emphasis on area averages of (a) SLP poleward of 60°N, (b) Z_{50} poleward of 65°N, and (c) total column ozone poleward of 40°N. The fraction of the recent trends in these time series that is linearly congruent with the AO time series is estimated on the basis of the methodology described in section 2, using monthly segments of the AO index. This fraction is shown only for those variables and months in which the trend in the AO is significant at the 90% level and year-to-year correlations of the variable in question with the AO index exceed the 95% significance level (both based on the t statistic taking into account the autocorrelation in the time series).

a. SLP

Table 4 shows linear 30-yr (1968–97) trends in the AO index (as defined in section 2) computed separately for each calendar month, in units of standard deviations of the monthly time series $(30\ \text{yr})^{-1}$. Positive trends are evident in all but two months of the year. However, trends exceeding the 95% significance threshold are ob-

TABLE 4. 30-yr (1968–97) linear trends in the AO index [(std dev (30 yr^{-1})]. Trends during JFM exceed the 95% significance threshold; trends during Aug exceed the 90% threshold.

Month	J	F	M	A	M	J	J	A	S	O	N	D
Trend	**+2.1**	**+2.6**	**+1.5**	−0.2	+0.2	+0.1	+0.3	**+0.6**	−0.1	+0.3	+0.7	+0.6

served only during January, February, and March. They exceed the 90% threshold during August.

Table 5 shows the corresponding 30-yr (1968–97) linear trends in SLP averaged over the polar cap region (60°–90°N) and the component of these trends that is linearly congruent with the monthly AO index. Consistent with the results of Walsh et al. (1996), the largest trends are evident during December–March, but falling pressures are evident during every month except April. The summertime trends, though relatively small, are of considerable interest, since the motion of the Arctic ice pack is believed to be most sensitive to wind forcing during that season (Serreze et al. 1989; Walsh et al. 1996). The summertime trends are also consistent with the results of Serreze et al. (1997), who noted sharp increases in spring and summer cyclone activity over the central Arctic since the mid-1980s, which in turn may be implicated in the recent reduction in sea ice cover along the Siberian coast (Maslanik et al. 1996). Our Tables 4 and 5 suggest that the springtime trends noted in these studies are dominated by the month of March. Large fractions of the trends during JFM and August are linearly congruent with the AO index (Table 5).

The structure of the SLP trends during the NH summer months (June–August; JJA) is shown in Fig. 10, together with the linearly congruent component based on the standardized leading principal component (PC) of NH JJA monthly mean SLP. The resemblance, though not as striking as in JFM, is still suggestive of a relationship with the AO.

b. Z_{50}

Table 6 shows analogous statistics for the 50-hPa height field averaged over the polar cap region (65°–90°N). Negative trends are evident in all months, with largest values from January through April. A large fraction of the Z_{50} drops during JFM is linearly congruent with the monthly AO index, but the drops during April are not mirrored in SLP. The summertime trends in the 50-hPa height field based on the NCEP–NCAR reanalysis (not shown) are weakly negative over most of the NH and are less concentrated over the polar cap region than in wintertime.

c. Ozone

The top two rows in Table 7 show analogous results for total column ozone trends averaged over the region poleward of 40°N, based on TOMS data. Values for November through February are omitted due to the limited coverage over the NH high latitudes. Negative trends are evident in all months of the year, with larger values during spring than later in the year. The delayed breakdown of the NH polar vortex has been linked to recent ozone depletion during this season (Newman et al. 1997; Hansen and Chipperfield 1998; Zhou et al. 1999). About 40% of the March ozone decrease is linearly congruent with the behavior of the AO, but the decrease later in the spring is not mirrored in SLP. These results are substantiated by the more extensive ozone record for Arosa, shown in the top two rows of Table 8.

While little, if any, of the late spring–early summer trends in ozone are linearly congruent with the AO index based on simultaneous correlations, it is conceivable that there could still be a causal linkage owing to the memory inherent in the ozone distribution. In order to illustrate this memory, we show in Fig. 11 time series of JFM and the subsequent JJA values of TOMS total column ozone averaged over the area poleward of 40°N. The resemblance is striking. The forward memory from March is further illustrated by the correlations in Table 9, which indicate that the memory of March total column ozone poleward of 40°N persists through the following summer. In contrast, there is little, if any ''backward memory''; that is, March ozone bears little relation to the ozone anomalies observed during the previous calendar year. If the autocorrelation inherent in the ozone field is taken into account, the season over which the declines in total column ozone can be viewed as linearly congruent with the AO index is extended into

TABLE 5. Top row: 30-yr (1968–97) linear trends in SLP (Z_{1000}) averaged over the NH polar cap region (60°–90°N) (m 30 yr^{-1}). Bottom row: The component of the trends that is linearly congruent with the monthly AO index. Total trends that exceed the 90% threshold are in bold type. The component of the trends that is linearly congruent with the AO index is shown only when 1) the appropriate monthly segments of the AO index are correlated with Z_{1000} at the 95% confidence level, and 2) the trend in the AO index exceeds the 90% confidence level (see Table 4).

	J	F	M	A	M	J	J	A	S	O	N	D
Trend	**−57**	**−56**	**−24**	+5	−7	−2	−5	**−14**	−1	−8	−8	**−24**
AO congruent	−43	−44	−30					−14				

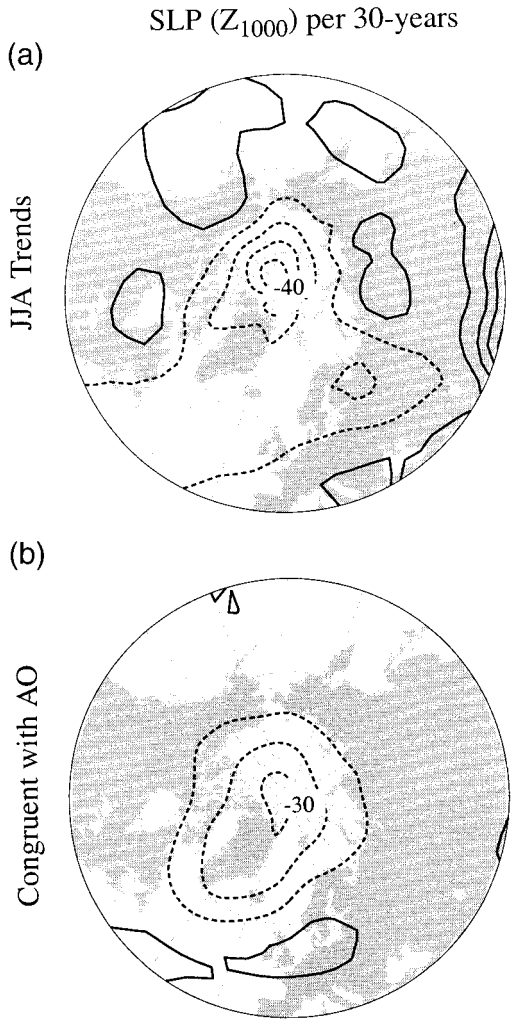

FIG. 10. (top) 30-yr (1968–97) linear JJA trends in SLP expressed as Z_{1000}. (bottom) The components of the trends that are linearly congruent with the monthly AO index. Contour intervals are 10 m per 30 yr (−15, −5, +5, . . .).

spring and summer, as illustrated in the third rows of Tables 7 and 8.

5. Trends in the Southern Hemisphere

As noted in Part I, the AO is remarkably similar to the primary annular mode in the extratropical SH general circulation. Like the AO, the SH mode is evident throughout the year in the troposphere. However, its active season in the lower stratosphere is observed during the late SH springtime when the SH polar vortex is decaying, rather than during midwinter, that is, in contrast to the NH, the SH active season occurs after, rather than before, the season of strongest ozone depletion.

There is increasing evidence that the SH annular mode, like the AO, has drifted toward the high index polarity during the past few decades. Tropospheric geopotential height has been falling over the Antarctic continent (Hurrell and van Loon 1994; Chen and Yen 1997; Meehl et al. 1998), and the SH polar lower stratosphere has cooled (and the SH polar vortex has strengthened) during the late springtime months (Trenberth and Olson 1989; Hurrell and van Loon 1994; Randel and Wu 1999). However, due to the paucity of observations over high latitudes of the SH and the questionable reliability of the trends in the NCEP–NCAR reanalysis in this region (e.g., see Randel and Wu 1999), it is difficult to estimate the component of the observed trends that is linearly congruent with the annular mode. Accordingly, we restrict our analysis in the SH to 1) documenting the seasonality of trends, and 2) establishing the similarity between the SH annular mode in the month-to-month variability and the observed trends.

a. SH troposphere

As in Part I, the annular mode in the SH is represented by the standardized leading PC time series of the 850-hPa height field poleward of 20°N, based on monthly mean data for all months of the year. Table 10 shows 30-yr trends in this index calculated independently for each calendar month. Positive trends, indicative of a strengthening of the westerlies at subpolar latitudes, are evident in all but one month. They exceed the 90% significance threshold during six calendar months, and no clear seasonality is evident.

b. Stratosphere

The trends in geopotential height in the stratospheric polar vortex exhibit a more pronounced seasonality than those in the lower troposphere. It is evident from Table 11 that the largest height falls have occurred during the active season (November) when the month-to-month variability of the annular mode is largest. Trends during the other months of the year are of mixed polarity. Trends in lower-stratospheric temperatures since 1979 based on MSU-4 data (Table 12) exhibit a qualitatively similar seasonality. Hence, despite our reservations concerning the reliability of the NCEP–NCAR reanalyses over this region, we consider these results to be at least qualitatively reliable.

TABLE 6. As in Table 5 but for Z_{50} averaged over the NH polar cap region (65°–90° N) [m (30 yr^{-1})].

	J	F	M	A	M	J	J	A	S	O	N	D
Trend	**−353**	**−202**	**−250**	**−144**	−11	**−31**	**−52**	**−59**	−14	**−64**	−37	−36
AO congruent	−246	−182	−118					−22				

TABLE 7. Top two rows: As in Table 5 but for 15-yr (November 1978–April 1993) trends in TOMS total column ozone averaged over the region 40°–90°N [DU (15 yrs^{-1})]. Bottom row: As in the middle row, but JFM seasonal mean values of the AO index are used in lieu of the contemporaneous AO index values. Values are omitted between Nov and Feb due to the absence of data over the high latitudes.

	J	F	M	A	M	J	J	A	S	O	N	D
Trend	—	—	**−49**	**−42**	**−26**	**−17**	**−11**	**−9**	**−10**	**−13**	—	—
AO congruent	—	—	−20								—	—
AO_{JFM} congruent	—	—	−22	−19	−14	−9	−6				—	—

The colder polar stratospheric temperatures during November have been linked to the tendency toward a delayed breakdown of the polar night jet (Hurrell and van Loon 1994; Zhou et al. 1999; Waugh et al. 1999; Waugh and Randel 1999), which has extended the length of the winter season by about two weeks. By analogy, the large interannual variability in November geopotential height and temperature may be a reflection of year-to-year differences in the timing of the breakdown of the jet. The corresponding trends in total column ozone averaged over the region poleward of 40°S are shown in Table 13. They are uniformly negative and exhibit a coherent seasonality with largest decreases in October. The ozone trends are more consistent from one calendar month to the next than the trends in 50-hPa height. This greater consistency derives, at least in part, from the strong month-to-month autocorrelation inherent in the ozone field, documented in Table 14. The forward memory from September is particularly strong.

Hurrell and van Loon (1994) have postulated that the trend toward a later breakdown of the SH stratosphere vortex has contributed to the observed ozone depletion. The strong resemblance between the spatial patterns of November ozone trends and the month-to-month variability of the annular mode, as documented in Fig. 12, is consistent with such an interpretation, as are the analogous NH relationships documented in the previous section. Since the strongest negative 50-hPa height tendencies over the polar cap region occur in November (Table 11), a month after the strongest ozone depletion (Table 13), at a time when the forward memory of the previous month's ozone is very strong (Table 14), any such dynamically induced ozone depletion would have to be viewed as a positive feedback occurring in response to chemically induced depletion earlier in the season.

6. Discussion and conclusions

a. Summary and interpretation of the observed trends

The results presented in section 3 serve to confirm and further document the remarkable correspondence between NH wintertime climate trends of the past few decades and the AO signature in the month-to-month variability. Both the trends and the AO are characterized by deep, barotropic, zonally symmetric signatures extending upward into the stratosphere, with embedded, baroclinic patterns that are largely confined to the troposphere. The 30-yr trend (1968–97) in the AO index for the months JFM amounts to 1.5 (2.1) standard deviations of the JFM month-to-month (JFM seasonal mean) variability in the index: enough to have had a substantial impact upon the NH general circulation during this period. Notable features of the trends that are integral parts of the AO signature during JFM include

- strengthening of the westerlies at subpolar latitudes coupled with weakening of the climatological mean jet stream at lower latitudes;
- warming of the lower troposphere over Eurasia and much of North America;
- cooling of the lower stratosphere in the polar cap region coupled with warming of the tropical tropopause; and
- a reduction in total column ozone poleward of 40°N.

The pronounced zonally symmetric zonal wind signature in the JFM trends is almost entirely linearly congruent with the month-to-month variability of the AO. The component of the zonally symmetric temperature trends that is not linearly congruent with the AO is dominated by amorphous tropospheric warming and stratospheric cooling reminiscent of the global warming signature as simulated in many climate models.

The sharply contrasting climate trends in various sectors of the NH pointed out by Hurrell (1995, 1996) are consistent with the trend in the AO toward the higher index polarity: that is, the milder winters in Eurasia (and particularly Siberia; Nicholls et al. 1996) juxtaposed against the trend toward more severe winters over eastern Canada (Shabbar et al. 1997); reduced precipitation in southern Europe and parts of the Middle East (Cullen and deMenocal 1999a, manuscript submitted to *Climatic*

TABLE 8. As in Table 7 but for 30-yr (1968–97) trends in total column ozone at Arosa, Switzerland [DU (30 yrs^{-1})].

	J	F	M	A	M	J	J	A	S	O	N	D
Trend	**−34**	**−59**	**−52**	**−48**	**−24**	**−28**	**−16**	**−19**	**−13**	**−13**	**−15**	**−29**
AO congruent	−16	−20	−16									
AO_{JFM} congruent	−19	−24	−24	−13	−11	−8	−5	−4				

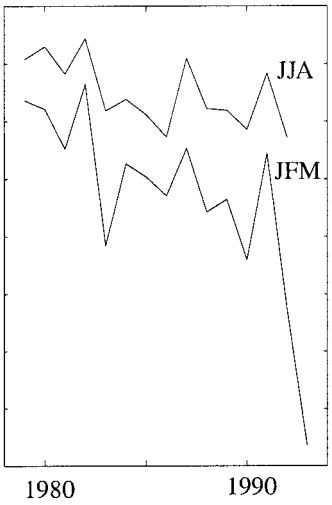

FIG. 11. Time series of total column ozone anomalies in DU averaged poleward of 40°N for (top) JJA and (bottom) JFM. Vertical tickmarks are at intervals of 10 DU. The time series have been plotted relative to different reference values to decrease the vertical spacing between them.

Change; Cullen and deMenocal 1999b, manuscript submitted to *Int. J. Climatol.*) and the retreat of Alpine glaciers (e.g., Frank 1997) juxtaposed against the trend toward heavier rainfall in northern Europe (e.g., Jones and Conway 1997) and advances of some northern European glaciers (Hagen 1995; Siggurdsson 1995). The trend toward higher wind speeds and wave heights over the far North Atlantic (Kushnir et al. 1997) and increasingly cyclonic wind stress around the Arctic that may, in turn, be responsible for some of the recent thinning and melting of the pack ice (McPhee et al. 1998) are also consistent with the recent trend in the AO.

The trend toward the positive polarity of the annular modes is consistent with observed changes in the stratospheric climatology in both hemispheres. The NH wintertime polar vortex is becoming colder, stronger, and less susceptible to midwinter warmings (Baldwin and Dunkerton 1999), and it is persisting later into the spring (Zhou et al. 1999; Waugh et al. 1999). In essence, the NH wintertime stratosphere climatology is becoming more like that of the SH, rendering it more susceptible to ozone destruction. The trends in the SH are not as pronounced, but the polar vortex is becoming established earlier in the autumn and persisting even later into the spring (Zhou et al. 1999; Waugh et al. 1999; Waugh and Randel 1999). In 1998 it remained intact, and ozone concentrations remained well below normal, until about a week before the summer solstice. The observed temperature and ozone trends are suggestive of an overall weakening of the wave-driven Lagrangian mean meridional circulation during JFM and November.

Our estimates of the component of the trends that is linearly congruent with the monthly AO index are slightly inflated due to the limited number of degrees of freedom inherent in the linear regression. If trends accounted for substantial fractions of the variance of the both the AO time series and the time series of the climatic variable in question, the apparent correlations between them would be strong simply by virtue of the shared trends, so the linearly congruent component would be estimated to be large, even in the absence of a statistically significant relationship between the time series. In the results presented in this paper, 30-yr trends account for only very small fractions of the variance of the AO time series and the various monthly climatic time series that enter into the trend estimates. We tested the sensitivity of our results to this possible source of bias by recalculating the linearly congruent part with the regression based upon detrended data. The results were found to be extremely robust. By far the largest sensitivities were encountered in the TOMS data because of the limited sample size: March means from 1979 to 1993. The trend in total column ozone poleward of 40°N over this period that is linearly congruent with the AO index drops from 40% to 30% if the regression is performed on detrended data. The corresponding reductions for total column ozone from Arosa and tropopause pressure from the NCEP–NCAR reanalysis amount to only a few percent.

b. Interpretation of the annular modes

Why is a single spatial structure so prominent in both Northern and Southern Hemispheres, in all seasons of the year, and across such a wide range of frequencies? Its pervasiveness may be due, in large part, to its high degree of zonal symmetry. Annular modes are characterized by a close alignment between the (anomalous) potential vorticity contours and the predominantly zonally symmetric background flow at all levels, so that strong local sources and sinks of heat and vorticity are not required to counteract local tendencies induced by advection, as is the case in more wavelike teleconnection patterns. A similar alignment between potential vor-

TABLE 9. Lag correlations (× 100) with respect to the month of Mar of year 0 for TOMS total column ozone anomalies averaged over the region 40°–90°N. Observations are not available over the polar night region between Nov and Feb.

	Year −1							Year 0							
Month	J	J	A	S	O	N	D	J	F	M	A	M	J	J	A
r	12	8	11	21	35					100	94	94	87	77	71

TABLE 10. 30-yr (1968–97) linear trends in the index of the SH annular mode [std dev 30 yr^{-1})]. Trends that exceed the 90% confidence level are in bold type.

	J	F	M	A	M	J	J	A	S	O	N	D
Trend	**+1.6**	+0.6	**+0.7**	**+0.9**	**+1.8**	0.0	+0.7	+0.8	+0.4	**+0.6**	+0.4	**+1.5**

ticity contours and streamlines is observed in long-lived blocking anticyclones.

What sets the meridional scale? Since the zonal wind perturbations in the annular modes are driven and maintained by the anomalous eddy fluxes of zonal momentum (Robinson 1991, 1996; Yu and Hartmann 1993; Feldstein and Lee 1998), it seems plausible that their meridional scale should be set by the climatology of the eddies that drive them. The fact that their nodal latitude occurs near 45° in both hemispheres, which corresponds roughly to the latitude of the strongest climatological mean poleward heat fluxes and eddy mixing, is consistent with this hypothesis. It is along this ''axis of symmetry'' of the eddies that perturbations in the momentum fluxes associated with the annular modes tend to be largest, both in the observations and in a realistic numerical simulation of both NH and SH annular modes (Limpasuvan and Hartmann 1999; 2000, manuscript submitted to *J. Climate*).

It may also be instructive to consider the relationship between the meridional structure of the annular modes in relation to the climatological mean, zonal-mean zonal wind field. It may be more than chance coincidence that the low index polarity of the annular modes is characterized by a well-defined ''subtropical'' jet stream ~35° lat, whereas in the high index polarity the subpolar jet is also a major player in the hemispheric circulation. The interplay between single and double jet ''regimes'' is reminiscent of numerical simulations of idealized atmospheres with planetary rotation rates comparable to that of the earth (e.g., Williams 1979; Lee 1997). The proximity of the latitude of the stratospheric polar night jet and the subpolar zonal wind perturbations associated with the annular modes allows for the possibility of vigorous interactions between troposphere and stratosphere during the active seasons. It seems plausible that perturbations in the annular modes originating at tropospheric levels should influence the evolution of the stratospheric polar vortex, and Hartley et al. (1998) have shown that dynamical processes operating at stratospheric levels can, through potential vorticity dynamics, induce a tropospheric response that projects strongly upon the annular mode.

To avoid confusing the NH annular mode (i.e., the AO) with the cold ocean–warm land (COWL) pattern defined by Wallace et al. (1995) or with the NAO (Hurrell 1995), it is worth pointing out what it shares in common with these two patterns and how it is distinct from each of them.

The AO's expression in surface air temperature projects strongly upon the COWL pattern over the North Atlantic, Eurasia, and eastern North America, while ENSO-like variability projects upon it over the Pacific and western North America. By construction, variations in the COWL pattern are more highly correlated with the high-frequency (month-to-month) variability of hemispheric-mean surface air temperature than any other pattern: that is the COWL pattern's one and only distinguishing characteristic. Unlike the AO or ENSO, the COWL pattern is not a naturally occurring mode of variability, recoverable in EOFs of observational data or control runs of GCMs, or even in one-point correlation maps (Broccoli et al. 1998). It closely resembles the observed SAT trends during 1968–97, which have been characterized by wintertime warming, not only over Eurasia but over Alaska and western Canada as well. The coincidence of strong wintertime warming in these two regions during this particular 30-yr period could well be fortuitous.

The NAO and the AO are different representations and conceptual interpretations of the same phenomenon (Kerr 1999; Wallace 2000). We prefer the AO for the following reasons.

1) The AO nomenclature conveys the notion that this pattern is an annular mode with a Southern Hemisphere counterpart (an ''Antarctic Oscillation''), both of which have relevance for stratospheric dynamics in their respective hemispheres, and for climate variability in regions far removed from the North Atlantic.
2) The AO representation is applicable to intraseasonal as well as interannual variability, whereas the NAO index used by Rogers (1984), Hurrell (1995, 1996), and others has to be averaged over entire winter seasons in order to obtain a meaningful represen-

TABLE 11. 30-yr (1968–97) linear trends in Z_{50} averaged over the SH polar cap region (65°–90°S) [m (30 yr^{-1})]. Trends that exceed the 90% confidence level are in bold type.

	J	F	M	A	M	J	J	A	S	O	N	D
Trend	−1	−3	+25	+16	**−99**	−24	+9	+66	**+77**	−64	**−206**	**−98**

TABLE 12. 19-yr (1979–97) linear trends in MSU4 temperature averaged over the SH polar cap region (65°–90°S) [K(19 yr^{-1})]. Trends that exceed the 90% confidence level are in bold type.

	J	F	M	A	M	J	J	A	S	O	N	D
Trend	**−0.5**	**−0.9**	**−1.0**	**−1.0**	−0.3	**−1.2**	−0.5	+1.2	+0.3	**−5.3**	**−6.5**	**−2.6**

tation of the corresponding planetary-scale circulation anomalies.

3) The AO time series exhibits a more significant trend: The positive trend in the NAO index for the months JFM during the period 1968–97 amounts to 0.9 (1.3) standard deviations of the monthly mean (JFM seasonal mean) time series; the corresponding statistic for the AO is 1.5 (2.1) standard deviations.
4) A larger fraction of the trends in most of the climatic fields considered here is linearly congruent with the month-to-month and season-to-season variability of the AO index than with the more commonly used NAO indices.

c. Remarks concerning possible causes of the trends

The above analysis indicates that more than one-third of the observed ozone depletion in the NH during JFM is linearly congruent with the AO and, owing to the high autocorrelation inherent in the ozone field, so is a substantial fraction of the depletion observed during the spring–summer months. In the SH, circulation changes associated with the drift toward the high index state of the annular mode peak sharply during November, whereas the ''ozone hole phenomenon'' occurs throughout a more extended spring season centered in October. Hence, the ozone destruction that begins around the time of the equinox each year must be photochemically induced, but positive feedbacks from the induced circulation changes may be allowing it to persist progressively later into the spring. The fact that summer ozone levels are highly correlated with ozone levels during the previous winter–spring on a year-to-year basis suggests that the summer–autumn ozone trends in both hemispheres are vestiges of the more pronounced depletion that has been taking place during the spring when the photochemistry and the dynamics are more active.

The month-to-month variability of the annular modes is largely internally generated, as evidenced by the fact that it is well simulated in control runs of a number of different atmospheric general circulation models run with fixed atmospheric composition (e.g., see Kitoh et al. 1996; Fyfe et al. 1999; Volodin and Galin 1998; Shindell et al. 1999; von Storch 1999; Limpasuvan and Hartmann 1999; 2000, manuscript submitted to *J. Climate*; Kidson and Watterson 1999; Gillet et al. 1999). Some of the interdecadal variations of these modes is sampling variability owing to the presence of these higher-frequency fluctuations. However, the recent trends during the active seasons emphasized in this paper stand out well above such background noise and they substantially exceed the interdecadal variability in the AO index prior to the 1970s.

Several different kinds of external forcing appear to be capable of inducing a response in the annular modes. In numerical experiments with general circulation models, Volodin and Galin (1998) obtained a distinctive AO-like wintertime response to radiative forcing designed to simulate the effects of stratospheric ozone depletion, and Shindell et al. (1999) and Fyfe et al. (1999) obtained similar responses to radiative forcing due to increasing concentrations of greenhouse gases and aerosols. In these simulations, forcing consistent with recent trends tended to drive the AO toward its high index polarity, consistent with observed trends. Robertson et al. (2000) reported that prescribing sea surface temperature variability over the North Atlantic in accordance with observations in a GCM simulation substantially increases the interannual variability of the AO, and Rodwell et al. (1999) showed that roughly half the decadal scale variance of the AO can be simulated as a response to the evolving pattern of Atlantic SST. The observed atmospheric response to volcanic eruptions during the boreal winter also resembles the AO, with elevated surface air temperatures over Eurasia (Robock and Mao 1992; Kodera 1994; Kelly et al. 1996) and below-normal SLP over the Arctic (Kelly et al. 1996). Hence, there is no shortage of mechanisms that might have contributed to the trend in the annular modes. It remains to be determined which of these should be viewed as the primary causal mechanism and which ones function as positive feedbacks that serve to amplify the response.

Acknowledgments. We would like to thank D. L. Hartmann, W. Randel, H. Nakamura, E. DeWeaver, and two

TABLE 13. 15-yr (November 1978–April 1993) linear trends in TOMS total column ozone averaged over the region 40°–90°S [DU (15 yrs^{-1})]. Observations are not available over the polar night region between May and Aug. Trends that exceed the 90% confidence level are in bold type.

	J	F	M	A	M	J	J	A	S	O	N	D
Trend	**−23**	**−17**	**−16**	**−16**					**−45**	**−57**	**−45**	**−35**

TABLE 14. Lag correlations (×100) with respect to Sep of year 0 for TOMS total column ozone anomalies averaged over the region 40°–90°S. Observations are not available over the polar night region between May and Aug.

Year −1								Year 0							
Month	F	M	A	M	J	J	A	S	O	N	D	J	F	M	A
r	39	39	51					100	95	92	88	80	78	73	63

reviewers (D. J. Karoly and J. W. Kidson) for their helpful comments and suggestions. Thanks also to D. Battisti, G. Bjarnason, P. Boynton, A. J. Broccoli, V. Dymnikov, P. Goodman, J. R. Holton, N.-C. Lau, P. Rhines, M. Serreze, D. Stephenson, and S.-P. Xie for insightful suggestions at various stages of this research. Two of the authors (DWJT and JMW) are supported by the National Science Foundation under Grant ATM-9805886. GCH was supported by the Alexander von Humboldt foundation and the National Science Foundation under Grant ATM-9707069.

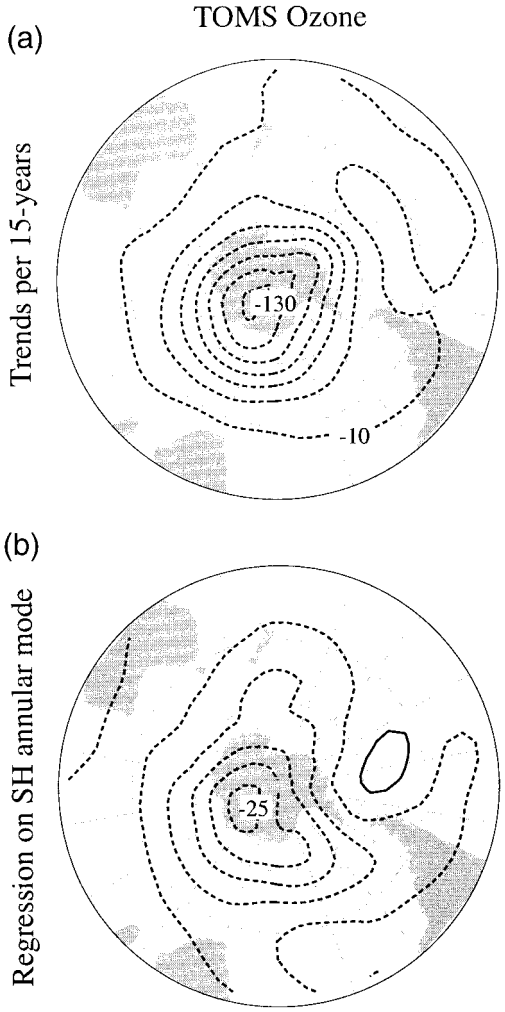

FIG. 12. (a) 15-yr (1978–1992) linear trends in November total column ozone. (b) Total column ozone regressed onto the index of the SH annular mode for the month of November. Contour intervals are 20 DU (15 yr)$^{-1}$ (−30, −10, +10, . . .) for the trends and 5 DU (−7.5, −2.5, 2.5, . . .) per std dev of the index for the regression map.

REFERENCES

Baldwin, M. P., and T. J. Dunkerton, 1999: Propagation of the Arctic Oscillation from the stratosphere to the troposphere. *J. Geophys. Res.,* **104,** 30 937–30 946..

Broccoli, A. J., N.-C. Lau, and M. J. Nath, 1998: The cold ocean-warm land pattern: Model simulation and relevance to climate change detection. *J. Climate,* **11,** 2743–2763.

Chen, T.-C., and M.-C. Yen, 1999: Interdecadal variation of the Southern Hemisphere circulation. *J. Climate,* **10,** 805–812.

Cubasch, U., G. C. Hegerl, and J. Waszkewitz, 1996: Prediction, detection and regional assessment of anthropogenic climate change. *Geophysica,* **32,** 77.

Dai, A., I. Y. Fung, and A. D. Del Genio, 1997: Surface observed global land precipitation variations during 1900–88. *J. Climate,* **10,** 2943–2962.

Feldstein, S. B., and S. Lee, 1998: Is the atmospheric zonal index driven by an eddy feedback? *J. Atmos. Sci.,* **55,** 3077–3086.

Frank, P., 1997: Changes of glacier area in the Austrian Alps between 1973 and 1992 derived from LANDSAT data. Max Planck Institute Report 242, Max Planck Institute for Meteorology, 21 pp.

Fyfe, J. C., G. J. Boer, and G. M. Flato, 1999: The Arctic and Antarctic Oscillations and their projected changes under global warming. *Geophys. Res. Lett.,* **26,** 1601–1604.

Gillet, N. P., G. C. Hegerl, M. R. Allen, and P. A. Scott, 1999: Implications of changes in hemispheric circulation for the detection of anthropogenic climate change. *Geophys. Res. Lett*., in press.

Graf, H.-F., J. Perlwitz, I. Kirchner, and I. Schult, 1995: Recent northern winter climate trends, ozone changes and increased greenhouse forcing. *Contrib. Atmos. Phys.,* **68,** 233–248.

Hagen, J. O., 1995: Recent trends in the mass balance of glaciers in Scandinavia and Svalbard. *Proc. Int. Symp. on Environmental Research in the Arctic*, Tokyo, Japan, National Institute of Polar Research, 343–354.

Hansen, G., and M. P. Chipperfield, 1999: Ozone depletion at the edge of the Arctic polar vortex 1996/1997. *J. Geophys. Res.*, **104,** 1837.

Hartley, D. E., J. T. Villarin, R. X. Black, and C. A. Davis, 1998: A new perspective on the dynamical link between the stratosphere and troposphere. *Nature,* **391,** 471–474.

Hulme, M., 1992: A 1951–80 global land precipitation climatology for the evaluation of general circulation models. *Climate Dyn.,* **7,** 57–72.

Hulme, M. 1994: Validation of large-scale precipitation fields in General Circulation Models. *Global Precipitations and Climate Change,* M. Desbois and F. Desalmand, Eds., NATO ASI Series, Springer-Verlag, 387–406.

Hurrell, J. W., 1995: Decadal trends in the North Atlantic Oscillation region temperatures and precipitation. *Science,* **269,** 676–679.

——, 1996: Influence of variations in extratropical wintertime teleconnections on Northern Hemisphere temperature. *Geophys. Res. Lett,* **23,** 665–668.

——, and H. van Loon, 1994: A modulation of the atmospheric annual cycle in the Southern Hemisphere. *Tellus,* **46A,** 325–338.

——, and ——, 1997: Decadal variations in climate associated with the North Atlantic Oscillation. *Climatic Change,* **36,** 301–326.

Jones, P. D., 1994: Hemispheric surface air temperature variations: A reanalysis and update to 1993. *J. Climate,* **7,** 1794–1802.
——, and D. Conway, 1997: Precipitation in the British Isles: An analysis of area-average data updated to 1995. *Int. J. Climatol.,* **17,** 427–438.
Kalnay, E. M., and Coauthors, 1996: The NCEP/NCAR Reanalysis Project. *Bull. Amer. Meteor. Soc.,* **77,** 437–471.
Kattenberg, A., and Coauthors, 1996: Climate models—Projections of future climate. *Climate Change 1995. The Second Assessment Report of the IPCC,* J. T. Houghton et al., Eds., Cambridge University Press, 285–359.
Kelly, P. M., P. D. Jones, and J. Pengqun, 1996: The spatial response of the climate system to explosive volcanic eruptions. *Int. J. Climatol.,* **16,** 537–550.
Kerr, R. A., 1999: A new force in high-latitude climate. *Science,* **284,** 241–242.
Kidson, J. W., and I. G. Watterson, 1999: The structure and predictability of the ''high-latitude mode'' in the CSIRO9 general circulation model. *J. Atmos. Sci.,* **56,** 3859–3873.
Kitoh, A., H. Koide, K. Kodera, S. Yukimoto, and A. Noda, 1996: Interannual variability in the stratospheric-tropospheric circulation in a coupled ocean-atmosphere GCM. *Geophys. Res. Lett.,* **23,** 543–546.
Kodera, K., 1994: Influence of volcanic eruptions on the troposphere through stratospheric dynamical processes in the Northern Hemisphere winter. *J. Geophys. Res.,* **99,** 1273–1282.
Kushnir, Y., V. J. Cardon, J. G. Greenwood, and M. A. Cane, 1997: The recent increase in North Atlantic wave heights. *J. Climate,* **10,** 2107–2113.
Lee, S., 1997: Maintenance of multiple jets in a baroclinic flow. *J. Atmos. Sci.,* **54,** 1726–1738.
Limpasuvan, V., and D. L. Hartmann, 1999: Eddies and the annular modes of climate variability. *Geophys. Res. Lett.,* **26**, 3133–3136.
Maslanik, J. A., M. C. Serreze, and R. G. Barry, 1996: Recent decreases in Arctic summer ice cover and linkages to atmospheric circulation anomalies. *Geophys. Res. Lett.,* **23,** 1677–1680.
McPhee, M. G., T. P. Stanton, J. H. Morison, and D. G. Martinson, 1998: Freshening of the upper ocean in the Arctic: Is perennial sea ice disappearing? *Geophys. Res. Lett.,* **25,** 1729–1932.
Meehl, G. A., J. W. Hurrell, and H. van Loon, 1998: A modulation of the mechanism of the semiannual oscillation in the Southern Hemisphere. *Tellus,* **50A,** 442–450.
Mitchell, J. F. B., and T. J. Johns, 1997: On modification of global warming by sulfate aerosols. *J. Climate,* **10,** 245–267.
——, R. A. Davis, W. J. Ingram, and C. A. Senior, 1995: On surface temperature, greenhouse gases, and aerosols: Models and observations. *J. Climate,* **8,** 2364–2386.
Newman, P. A., J. F. Gleason, R. D. McPeters, and R. S. Stolarski, 1997: Anomalously low ozone over the Arctic. *Geophys. Res. Lett.,* **24,** 2689–2692.
Nicholls, N., G. V. Gruza, J., Jouzel, T. R. Karl, L. A. Ogallo, and D. E. Parker, 1996: Observed climate variability and change. *Climate Change 1995. The Second Assessment Report of the IPCC,* J. T. Houghton et al., Eds., Cambridge University Press, 133–192.
Parker, D. E., C. K. Folland, and M. Jackson, 1995: Marine surface temperature: Observed variations and data requirements. *Climatic Change,* **31,** 559–600.
Randel, W. J., and F. Wu, 1999: Cooling of the Arctic and Antarctic polar stratospheres due to ozone depletion. *J. Climate,* **12,** 1467–1479.
——, ——, J. M. Russell III, and J. Waters, 1999: Space-time patterns of trends in stratospheric constituents derived from UARS measurements. *J. Geophys. Res.,* **104,** 3711–3727.
Robertson, A. W., C. R. Mechoso, and Y.-J. Kim, 2000: The influence of Atlantic sea surface temperature anomalies on the North Atlantic Oscillation. *J. Climate,* in press.
Robinson, W. A., 1991: The dynamics of the zonal index in a simple model of the atmosphere. *Tellus,* **43A,** 295–305.
——, 1996: Does eddy feedback sustain variability in the zonal index? *J. Atmos. Sci.,* **53,** 3556–3569.
Robock, A., and J. Mao, 1992: Winter warming from large volcanic eruptions. *Geophys. Res. Lett.,* **19,** 2405–2408.
Rodwell, M. J., D. P. Rowell, and C. K. Folland, 1999: Oceanic forcing of the wintertime North Atlantic Oscillation and European climate. *Nature,* **398,** 320–323.
Rogers, J. C., 1984: Association between the North Atlantic Oscillation and the Southern Oscillation in the Northern Hemisphere. *Mon. Wea. Rev.,* **112,** 1999–2015.
Serreze, M. C., R. G. Barry, and A. S. McLaren, 1989: Seasonal variations in sea ice motion and effects of sea ice concentration in the Canada Basin. *J. Geophys. Res.,* **94,** 10 955–10 970.
——, F. Carse, R. G. Barry, and J. C. Rogers, 1997: Icelandic low cyclone activity: Climatological features, linkages with the NAO, and relationships with recent changes in the Northern Hemisphere circulation. *J. Climate,* **10,** 453–464.
Shabbar, A., K. Higuchi, W. Skinner, and J. L. Knox, 1997: The association between the BWA index and winter surface temperature variability over eastern Canada and west Greenland. *Int. J. Climatol.,* **17,** 1195–1210.
Shindell, D. T., R. L. Miller, G. Schmidt, and L. Pandolfo, 1999: Simulation of recent northern winter climate trends by greenhouse-gas forcing. *Nature,* **399,** 452–455.
Siggurdson, O., and T. Jonsson, 1995: Relation of glacier variations to climate changes in Iceland. *Ann. Glaciol.,* **21,** 263–270.
Spencer, R. W., and J. R. Christy, 1993: Precision lower stratospheric temperature monitoring with the MSU: Technique, validation, and results 1979–1991. *J. Climate,* **6,** 1194–1204.
Staehelin, J., and Coauthors, 1998: Total ozone series at Arosa (Switzerland): Homogenization and data comparison. *J. Geophys. Res.,* **103,** 5827–5841.
Steinbrecht, W., H. Claude, and U. Kohler, 1998: Correlations between tropopause height and total ozone: Implication for long-term changes. *J. Geophys. Res.,* **103,** 19 183–19 192.
Thompson, D. W. J, and J. M. Wallace, 1998: The Arctic Oscillation signature in the wintertime geopotential height and temperature fields. *Geophys. Res. Lett.,* **25,** 1297–1300.
——, and ——, 2000: Annular modes in the extratropical circulation. Part I: Month-to-month variability. *J. Climate,* **13,** 1000–1016.
Trenberth, K. E., and D. A. Paolino, 1980: The Northern Hemisphere sea level pressure dataset: Trends, errors and discontinuities. *Mon. Wea. Rev.,* **108,** 855–872.
——, and J. G. Olson, 1989: Temperature trends at the South Pole and McMurdo Sound. *J. Climate,* **2,** 1196–1206.
——, and J. W. Hurrell, 1994: Decadal atmospheric-ocean variations in the Pacific. *Climate Dyn.,* **9,** 303–309.
Volodin, E. M., and V. Ya. Galin, 1998: Sesitivity of midlatitude Northern Hemisphere winter circulation to ozone depletion in the lower stratosphere. *Russ. Meteor. Hydrol.,* **8,** 23–32.
von Storch, J.-S., 1999: On the reddest atmospheric modes and the forcings of the spectra of these modes. *J. Atmos. Sci.,* **56,** 1614–1626.
Wallace, J. M., 2000: North Atlantic Oscillation/Annular Mode: Two paradigms—One phenomenon. *Quart. J. Roy. Meteor. Soc.,* in press.
——, Y. Zhang, and J. A. Renwick, 1995: Dynamic contribution to hemispheric mean temperature trends. *Science,* **270,** 780–783.
Walsh, J. E., W. L. Chapman, and T. L. Shy, 1996: Recent decrease of sea level pressure in the central Arctic. *J. Climate,* **9,** 480–486.
Waugh, D. W., and W. J. Randel, 1999: Climatology of Arctic and Antarctic polar vortices using elliptical diagnostics. *J. Atmos. Sci.,* **56,** 1594–1613.

——, W. J. Randel, S. Pawson, P. A. Newman, and E. R. Nash, 1999: Persistence of the lower stratospheric polar vortices. *J. Geophys. Res.,* **104,** 27 191–27 202.

Williams, G. P., 1979: Planetary circulations. Part III: Terrestrial quasi-geostrophic regime. *J. Atmos. Sci.,* **36,** 1409–1435.

World Meteorological Organization, 1995: Scientific assessment of ozone depletion: 1994. WMO Report 37, Geneva, Switzerland.

Yu, J.-Y., and D. L. Hartmann, 1993: Zonal flow vacillation and eddy forcing in a simple GCM of the atmosphere. *J. Atmos. Sci.,* **50,** 3244–3259.

Zhang, Y., J. M. Wallace, and D. S. Battisti, 1997: ENSO-like interdecadal variability: 1900–93. *J. Climate,* **10,** 1004–1020.

Zhou, S., M. E. Gelman, A. J. Miller, and J. P. McCormack, 1999: An inter-hemisphere comparison of extended winter conditions in the stratosphere. *Proc. 10th Symp. on Global Change Studies,* Dallas, TX, Amer. Meteor. Soc., 141–142.